DeepCwind Semi-Submersible Floating Offshore Wind Turbine Platform with Nonlinear Multi-Segment Catenary Mooring Line and Intermediate Buoy

Mohammad Motallebi, Hassan Ghassemi*
Department of Maritime Engineering, Amirkabir University of Technology, Tehran, Iran.
* Corresponding author: E-mail: gasemi@aut.ac.ir
Website: http://hmaa.itgo.com/ghassemi.html

Abstract
In this paper, with the purpose of improving the mechanical behavior of DeepCwind semi-submersible floating offshore wind turbine (FOWT) platform mooring lines, nonlinear catenary cables of platform are divided into multi-segments and intermediate buoy. The mathematical formulations of the dynamic equation acted on the cable with buoys are described. Present study is employed to the OC4-DeepCwind semi-submersible FOWT platform. It is designed for 200-meter water depth with mooring lines consist of three catenary steel chain cables that have an angle of 120 degrees to each other. The dynamic response of multi-segment catenary mooring line with different buoys radiuses and different positions along the cables were investigated. The full-scale platform was modeled in ANSYS-AQWA software and the simulations are performed in harsh offshore. The tension, strain, anchor uplift, cable uplift for different buoy radiuses and its position along cable are presented and discussed. Moreover, platform motions at three directions (surge, heave and pitch) are also analyzed. It is concluded that by correct selection of the buoy volume and position along cable, the tension of the cable may be reduced up to 45%. By incorrect selection of the buoy, the results will cause adverse effects.

Keywords:
Semi-submersible floating platform, Offshore wind turbine, Dynamic response, Catenary mooring system, Intermediate buoy, Strain and tension.

1. INTRODUCTION

Semi-submersible floating platforms are nowadays the most common deep-water sub-structures for FOWT. Mooring of floating units is one of the most important parts of design and erection of these floating platforms in deep water. In which according to Bae's investigations, failure of one cable of OC4-DeepCwind semi-submersible FOWT's mooring line can result in over 700 [m] drift, which can lead to damage other structures in offshore wind farms [1]. In the semi-submersible drilling Platform for safe operation and preventing damage to excavation's equipment, the horizontal movements of the platform are limited to less than one percent of water depth, where the major restriction of horizontal responses is provided by mooring lines [2]. Full-scale fatigue assessment testing of catenary steel chain mooring under tensile loads was performed by Martinez et al. [3] in similar saline water conditions. The purpose was to predict the fatigue lifetime and identify the locations of fatigue failure in the chains. It has been found that chain failure often occurs at the point of the intrados (KT point) and crown zones, because of further concentration of localized stresses in these areas. Hence, the investigation of the resulting forces and mechanical behavior of mooring lines of semi-submersible floating wind turbine platforms to derive a safely condition and prevent potential of risks, has always been a major concern. Hall and Goupee [4] simulated DeepCwind semi-submersible FOWT system including mooring dynamics. They introduced a lumped-mass mooring line model and validated it against

test data of scale-model floating offshore wind turbine. Azcona et al. [5] developed a code for dynamic response of mooring lines base on finite element with three translational degrees of freedom in each nodes of lumped mass. A new frequency domain modeling approach presented for FOWT with coupled wind turbine, floating platform, and mooring system sub-models. The sub-models are generated using the validated numerical tools FAST and WAMIT to obtain the frequency domain aerodynamic and hydrodynamic characteristics, respectively, for any given design candidate [6]. Low-frequency drift effect should be considered when TLP loses tendons. The in-plane second-order hydrodynamic loads attain approximately 10% to maximum of 40% of total horizontal loads. This phenomenon leads to magnify TLP's horizontal offset and rotation [7]. Lee et al. [8] explored the causes of the mooring system's failure of a typical marine vessel. Then, using the results of dynamic and static analyses, an equation to predict exert tension of mooring lines was presented. They could increase the safely factor against fairlead mooring failure by using bitt foundation plate and bolts at fairlead point.

Since the semi-submersible DeepCwind platform mooring line system usually consist of steel chains, [9] the benefits of this system in comparison to other materials such as wire or synthetic ropes, include easy installation, convenient repair, lower installation cost, high resistance against abrasion or marine growth, and high stability against offset due to high dead weight. On the other hand, the disadvantages of this mooring system include low elasticity and intermediate fatigue resistance. Also, as the depth of water increases, the weight of chains becomes too large and the vertical forces due to the weight of the cables which apply to the float, will increase. Consequently, due to the increase of the weight, costs also increase and makes the system economically infeasible, although it increases the capacity of system against exert forces. The benefits of using buoy in the deep-water catenary mooring system can include weight loss of a heavy chain and wire of mooring system, reduction of pre-tension and element strain along cable as well as reducing the cable's weight and radius of containment, which results in lowering the construction costs and enhancing the operation safety. There are advantages and disadvantages of applying buoys in catenary mooring line. The advantages are to reduce the weight of heavy chain and wire, and decrease the pre-tension. It is also caused to diminish the mooring radius, and decrease the influence of other cable installation. Third advantage is the deposit part of restoring force, and capability to resist more harsh ocean loads. Meanwhile, the disadvantages of applying buoys in catenary mooring line are to increase the installation process, and induce the risk of buoys damage, and to cause more complex dynamic characteristics of hybrid mooring line. Figure 1 shows the semi-submersible FOWT platform and mooring line system.

The idea of using buoys in the mooring line systems has attracted the attention of researchers. Static analysis of the chain cables with buoy was investigated by Dongjiao [10] to determine the effect of buoy's size and weight of buoy on cables' tension. Qiao et al [11] carried out numerically the effect of buoys on the dynamics pf mooring systems and motion response of platform. Ghaffari and Dardel, [12] examined the effect of diameter and number of buoys on the response of the Amirkabir semi-submersible drilling platform. The results show that with increasing the number of buoys, the time domain response amplitude of surge motion is reduced, also in heave and pitch motions the amplitude of oscillations is increased. Kwan and Bruen, [13] compared the dynamic calculation methods, including the frequency domain, the time domain, and the quasi-static methods using numerical simulation, and recommended using the time domain method for nonlinear dynamic analysis of cables with buoys. The attached buoys could reduce the tension on the mooring lines. This is a significant improvement for the mooring system since it provides a good approach to solve the contradiction between the vessel's motion and the lines' tension [14]. For this reason, this paper is to investigate the influence of buoys

with different dimensions and its positions to obtain the configuration for depreciating the tension, elements strain and uplift of mooring lines without noticeable altering the DeepCwind FOWT motions in harsh offshore environmental conditions.

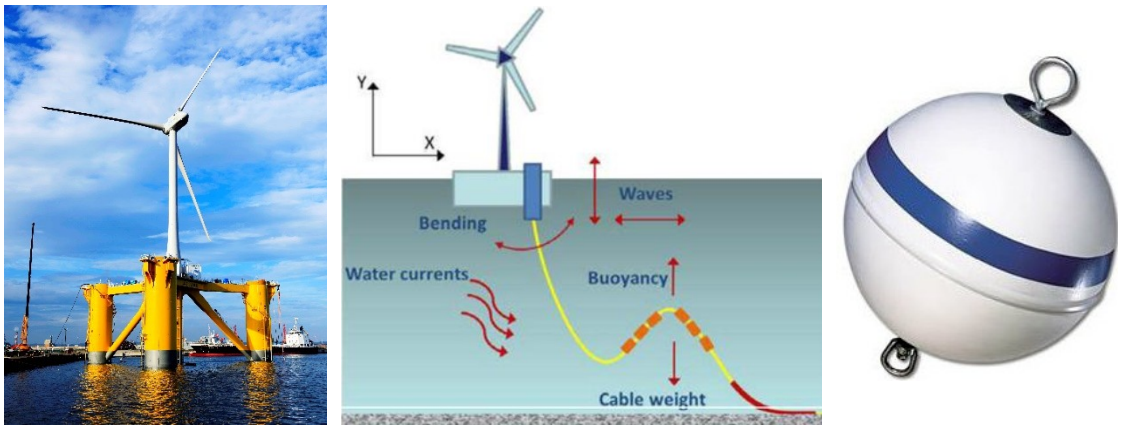

a) OC4-DeepCwind semi-submersible FOWT platform

b) Semi-submersible FOWT and mooring line

c) Spherical buoy

Figure 1. Semi-submersible FOWT platform with mooring line and buoy

The rest of this paper is structured as follows. Section 2 describes the mathematical formulations of the dynamic of catenary mooring lines and the dynamic of multi-segment catenary mooring line with intermediate buoys. The methodology applied to obtain the results are presented in Section 3. Section 4 is given the comparison of the numerical results and experimental data for the platform motions and fairlead tension. More numerical results of the platform motion, cable strain, cable tension, anchor uplift at different buoy radiuses and positions are presented and discussed in Section 5. Finally, some concluding remarks are presented in Section 6.

2. MATHEMATICAL FORMULATIONS

2.1. Dynamic of catenary mooring lines

In order to analyze of the dynamics of the cable motion, many factors are required to consider such as the effects of cable mass, drag forces, inline elastic tension and bending moment. The forces applied to the cable vary with time and generally the cables behave nonlinearly. The simulation of cable dynamics is needed to discretize cable along its length and assemble the mass and applied forces. Each mooring line is discretized in a spring-mass chain of *N* Morison-type elements [15] subjected to various external forces, as shown in Figure 2. The general equations for the force and moment acted to the cable are expresses as follows:

$$\frac{\partial \vec{T}}{\partial S_e}+\frac{\partial \vec{V}}{\partial S_e}+\vec{w}+\vec{F}_h=m\frac{\partial^2 \vec{R}}{\partial t^2}$$

$$\frac{\partial M}{\partial S_e}+\frac{\partial R}{\partial S_e}\times\vec{V}=-q \qquad (1)$$

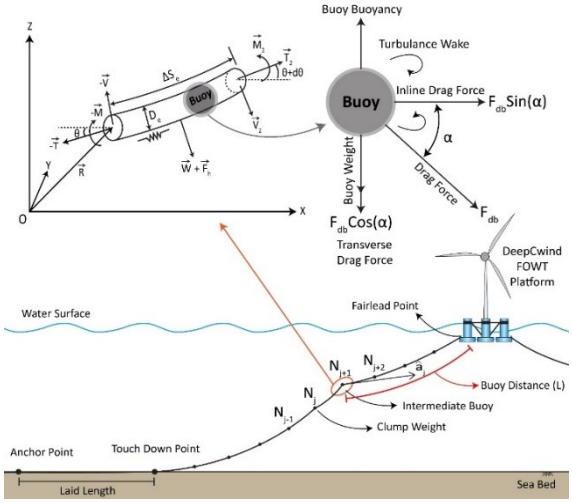

Figure 2. Modeling of dynamic cable with intermediate buoy

where *m* is the mass of cable element per unit length, $\vec{q}$, $\vec{V}$,$\vec{M}$, $\vec{T}$, $\vec{R}$ are distributed moment, shear force, bending moment, tension force and position vectors of the first node from the cable element, respectively. S_e is the partial length of the element, also $\vec{F_h}$ and $\vec{w}$ are the external hydrodynamic forces and weight vectors per unit length, respectively.
The bending moment (*M*) depends on bending stiffness (EI), and the tension force (*T*) is dependent on the axial stiffness of cable material (EA) and the axial strain of elements (ε). The tension force and bending moment are defined as follows:

$$M = EI \frac{\partial R}{\partial S_e} \times \frac{\partial^2 R}{\partial S_e^2} \qquad (2)$$

$$T = EA\,\varepsilon$$

In order to determine the cable's dynamic response, the elements of the cable are converted into the number of concentrated masses, and the equations in each node were numerically solved. We choose two pinned points at top($\vec{P}_{top}$) and bottom ($\vec{P}_{bottom}$) of the unstretched cable (L) as boundary conditions, which are given as follows:

$$R(0) = P_{bottom}, \quad R(L) = P_{top}$$

$$\frac{\partial^2 R(0)}{\partial S_e^2} = 0 \quad \frac{\partial^2 R(L)}{\partial S_e^2} = 0 \qquad (3)$$

The unit axial vector of *j-th* element which is related to the slope of two adjacent elements, is equal $\hat{a}_j = \frac{\vec{R}_{j+1} - \vec{R}_j}{L_j}$, so the unstretched element length with a good approximation is $S_{ej} \approx L_j = \left|\vec{R}_{j+1} - \vec{R}_j\right|$. Therefore, the curvature vector at point *j* ($\vec{C}_j$) is defined by the rate of slope change which is calculated from the cross product of unit vectors of the two adjacent elements. $\vec{L}_j$ is the effective length of the *j*-th node which defines as $\overline{L}_j = \frac{L_j + L_{j-1}}{2}$.

$$\vec{C}_j = -\frac{\partial R}{\partial S_e} \times \frac{\partial^2 R}{\partial S_e^2}\bigg|_j = \frac{1}{\overline{L}_j}\hat{a}_j \times \hat{a}_{j-1} \tag{4}$$

With assuming the bending stiffness (EI) is constant between two adjacent elements, then the Eqs. (2) and (4) lead to the bending moment at point *j* results is found by

$$M_j = -(EI)_j C_j \tag{5}$$

Let's define the axial (A_j) and normal (N_j) directional tensors as follows:

$$\begin{aligned} A_j &= \hat{a}_j^T \hat{a}_j \\ N_j &= I - A_j \end{aligned} \tag{6}$$

For the general configuration of cables, the axial stiffness (EA) is much greater than the bending stiffness(EI), so assuming the distributed bending moment is zero, from Eqs. (1) and (6), the shear force matrix on the element *j* is expressed as

$$\left[V_{(j)}\right] = -\frac{1}{L_j} N_j \left[(EI)_{j+1} \frac{1}{L_{j+1}} \hat{a}_{j+1} + (EI)_j \frac{1}{L_j} \hat{a}_{j-1}^T \right] \tag{7}$$

The element bending stiffness matrix is obtained by directly deriving from the shear force as Eq. (8).

$$\left[dV\right] = \left[\nabla^T V\right]^T \left[u\right] = -K_b \left[u\right] \tag{8}$$

From Eq. (7) it can be seen that the shear force on element *j* is a function of the four-node positions of *j-1, j, j+1* and *j+2* (for the elevation of $\hat{a}_{j-1}$ and $\hat{a}_{j+1}$, which defined by $\hat{a}_j = \frac{\vec{R}_{j+1} - \vec{R}_j}{L_j}$). Accordingly, K_b is a 12×12 matrix. Indicating $[u_{j-1}], [u_j], [u_{j+1}], [u_{j+2}]$ as the motions at these four points, by substituting Eq. (7) into Eq. (8), it is expressed as follows:

$$\left[dV_{(j)}\right] = \sum_{m=j-1}^{j+2} \left[\nabla^T \vec{V}\right]^T \left[u_m\right] = \sum_{m=j-1}^{j+2} -K_m \left[u_m\right] \tag{9}$$

where:

$$K_m^T = \frac{1}{L_j}\left[\Xi_j \nabla_m\right]^T A_j + (\nabla_m^T \frac{1}{L_j})\Xi_j^T N_j + \frac{1}{L_j}(\nabla_m^T \Xi_j^T) N_j \tag{10}$$

Concerning the displacement at node *m*, $\nabla_m = (\frac{\partial}{\partial x}, \frac{\partial}{\partial y}, \frac{\partial}{\partial z})\big|_m$ is the gradient operator and Ξ_j is defined as

$$\Xi_j = -\left\{ (EI)_{j+1} \frac{1}{\overline{L}_{j+1}} \left[\hat{a}_{j+1} - \hat{a}_j \right]^T - (EI)_j \frac{1}{\overline{L}_j} \left[\hat{a}_j - \hat{a}_{j-1} \right]^T \right\} \tag{11}$$

The axial elastic force applied to the element (j) is defined as a function of two-node deformation in the following form

$$-K_a \begin{bmatrix} [u_j] \\ [u_{j+1}] \end{bmatrix} = dF \tag{12}$$

where K_a is the 2×2 stiffness matrix of the mooring line element characterized as

$$K_a = \begin{bmatrix} K_{33} & -K_{33} \\ -K_{33} & K_{33} \end{bmatrix}, \text{where } K_{33} = K_x A_j + \frac{T_j}{L_j} N_j \tag{13}$$

Providing K_x is the inline linear stiffness or equivalent inline stiffness for a nonlinear axial stiffness cable. By bringing the all elements matrices together and applying boundary conditions on the two attachment points of the mooring line, the static solution can be solved as

$$K \left[u \right] = F_{total} \tag{14}$$

In time domain analysis, cable motion at the given attachment locations can be obtained by

$$M \left[\ddot{u} \right] = F_{total} \tag{15}$$

2.2. Dynamic of multi-segment catenary mooring line with intermediate buoy

By integrating both sides of Eq. (1) and applying the boundary conditions at the cable's ends, the *j-th* element motion response can be written as the matrix form:

$$\begin{bmatrix} -T_j \hat{a}_j^T \\ -T_{j+1} \hat{a}_j^T \end{bmatrix} + \begin{bmatrix} -[V_j] \\ [V_{j+1}] \end{bmatrix} + \frac{L_j}{2} \begin{bmatrix} [w + F_h]^T \\ [w + F_h]^T \end{bmatrix} = \frac{mL_j}{2} \frac{\partial^2}{\partial t^2} \begin{bmatrix} R_j^T \\ R_{j+1}^T \end{bmatrix} \tag{16}$$

It is noted that the j in the parentheses represents the element and without parenthesis represents the node. As respects $[V_j] = [V_{(j-1)}] - [V_{(j)}]$ is the shear force at node j, which is obtained by discretizing two adjacent elements. F_h is applied hydrodynamic forces on cable which consist of buoyancy force (F_b¿ and Morison force for the inline forces caused by the vibration of the body under the stimulation of the wave and the current. Morrison's force is divided into two parts of drag $(F¿¿d)$¿and radiation force $(F¿¿r)$¿. The radiation force depends on the cable element added mass matrix $(m¿¿a)$¿ and acceleration of the cable ($\vec{a}_j$) at node j. The general form of hydrodynamic forces is given by following equation:

$$F_h = F_b + F_d - m_a \left[\vec{a}_j, \vec{a}_{j+1} \right]^T \tag{17}$$

If the mass of an intermediate clump weight attached at node j is defined by M, and if there is no clump weight at the $j+1$ node, total gravitational force in the element with the starting and ending nodes of j and $j+1$, is a 6×1 matrix in the fixed references axes. Assuming half of the gravitational force caused by the clump weight affects the adjacent element. g is gravitational acceleration, the clump weight at node j and $j+1$ are given as follows:

$$w = (\vec{w}_j, \vec{w}_{j+1})^T = \left\{0,0,-\frac{1}{2}(mL_j + M)g, 0,0,-\frac{1}{2}mL_j g\right\}^T \tag{18}$$

Assuming that there is a clump weight at node j and an intermediate buoy at node $j+1$. Indicating the displaced mass of water of intermediate buoy as M_b, and the equivalent cross-sectional area of mooring line as A_{cj}, the element buoyancy force matrix is defined as

$$F_b = \left\{0,0,\frac{1}{2}\rho_w A_{cj} L_j g, 0,0,\frac{1}{2}(\rho_w A_{cj} L_j + M_b)g\right\}^T \tag{19}$$

where ρ_w is the density of water. The simplified form of the drag force applied to the mooring lines element in the time domain is given by

$$F_d(t) = \begin{Bmatrix} f_d(j) - \frac{1}{2}C_{dc}S_c\rho_w \left|U_j(t) - V_j(t)\right|\left\{U_j(t) - V_j(t)\right\} \\ f_d(j+1) - \frac{1}{2}C_{db}S_b\rho_w \left|U_{j+1}(t) - V_{j+1}(t)\right|\left\{U_{j+1}(t) - V_{j+1}(t)\right\} \end{Bmatrix} \tag{20}$$

Here $V_j(t) = \left\{V_{x_j}(t), V_{y_j}(t), V_{z_j}(t)\right\}^T$ is the shape matrix of mooring line velocity at node j at time t, $U_j = U_j^T = \left\{U_{xj}, U_{yj}, 0\right\}^T$ is the matrix form of the current velocity at the location of node j. C_{dc} and C_{db} are the drag coefficient of the clump weight (attached at node j) with projected surface areas of S_c and the intermediate buoy (attached at node $j+1$) with projected surface areas of S_b, respectively. The drag force on the mooring line element $(f_d(j))$ is expressed as

$$\begin{aligned} f_d(j) = &-\frac{1}{4}C_x\rho_w D_j L_j \left|A_j\left\{U_j(t) - V_j(t)\right\}\right| A_j\left\{U_j(t) - V_j(t)\right\} \\ &-\frac{1}{4}C_d\rho_w D_j L_j \left|N_j\left\{U_j(t) - V_j(t)\right\}\right| N_j\left\{U_j(t) - V_j(t)\right\} \end{aligned} \tag{21}$$

where C_d and C_x are the transverse and inline drag coefficients, respectively.

In order to obtain the proper results, the drag force along the cable element should be integrated to consider the variation of current velocity along the element. In this paper, the Gaussian numerical integration method is used to calculate this integral.

3. METHODOLOGY OF RESEARCH

In this research, the process of study is based on OC4-DeepCwind semi-submersible FOWT platform [9]. Numerous experiments have been carried out by using the 5 MW baseline wind turbine developed by NREL [16] [17] [18]. An overview of the NREL-FAST structure including the various modules and datasets of input and output analysis process is provided by Imani et al. [19]. The platform is designed for 200-meter water depth. The mooring lines consist of three catenary steel chain cables that have an angle of 120 degrees to each other, depicted in Figure 3. Table 1 shows the specifications of the mooring lines.

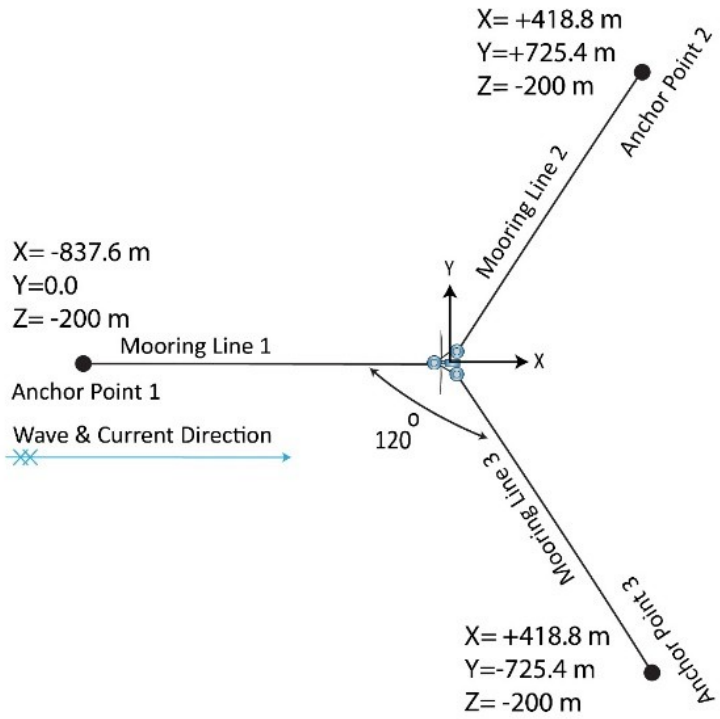

Figure 3. Plan of mooring system and anchor points coordinations

Table 1. Mooring line properties

Unstretched Mooring Line Length [m]	835.5
Radius to Anchors from Platform Centerline [m]	837.6
Chain Diameter [m]	0.0766
Equivalent Mass per Unit Length (kg/m)	108.63
Axial Stiffness (EA) (N)	753600000
Tensile Strength (N)	5454000
Longitudinal Drag Coefficient	0.025

To improve the performance of DeepCwind mooring line system, catenary cables divided into two different segmentations and an intermediate buoy was attached at the catenary segment joints. The material properties of cable are considered the same on both sides of the joint. Six spherical buoys device with different radiuses (seven radiuses) of 0.8, 1.0, 1.2, 1.4, 1.6, 1.8 and 2.0 meter with different added mass, displaced water and drag coefficient were selected. The reasons for choosing high volume of buoys, is to provide horizontal stiffness to prevent large offset of the platform [20]. Each of these buoys individually connected along three cables at six distance of 100, 200, 300, 400, 500 and 600 meters from fairlead point. The cables convert into two different segments and the buoy is in the intersection joint of it. Figure 4 shows the

configuration of mooring lines by arranging different buoys simultaneously at different distances. The difference between the sizes of buoys on the mooring system configuration is well illustrated. The buoys at the joints have positively raised the cable. The greater radius of buoy, due to the increase in buoyancy and bearing part of the cable weight, it will increase positive rise further. Also, as the buoy gets closer to the anchor point, the angle of joint segments increases. In this figure, "R" represents the radius of buoys and "L" indicates the horizontal distance between the center of buoy to fairlead point on platform. The full-scale platform was modeled in ANSYS-AQWA software and the simulations are performed in harsh offshore conditions with the 50-year return period load cases based on ultimate limit state (ULS) design criteria shown in Table 2. This simulation based on boundary element method (BEM) is conducted by utilizing three-dimensional radiation/diffraction theory and Morison's equation (hybrid method) in regular waves in the frequency and time domain.

Table 2. Environmental conditions

Wave Properties	
Wave Type	Stokes 2nd Order Wave Theory
Propagation Direction	0^0 (Parallel to Turbine Hub)
Wave Height (m)	8
Period (s)	9.43
Frequency (Hz)	0.106
Current Properties	
Distribution method	Exponentially in Depth
Propagation Direction	0^0 (Parallel to Turbine Hub)
Variation Inverse Exponent	2
Velocity at free surface of water (m/s)	1.06
Velocity at Depth of 100 meter (m/s)	0.75

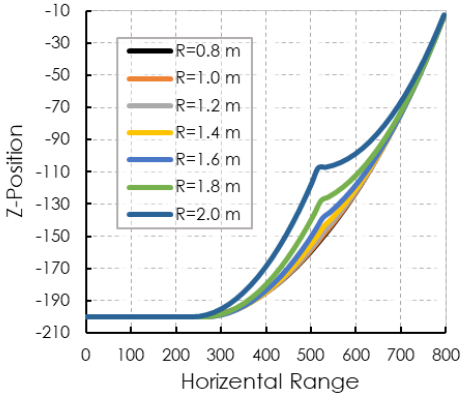

b) Buoy distance from fairlead (L) =300 m

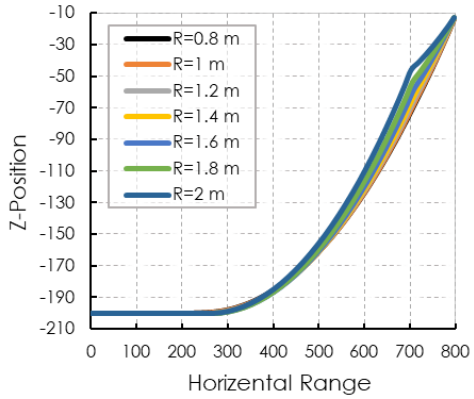

a) Buoy distance from fairlead (L) =100 m

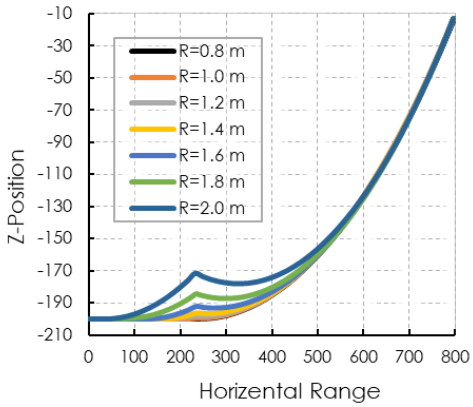

d) Buoy distance from fairlead (L) =600 m

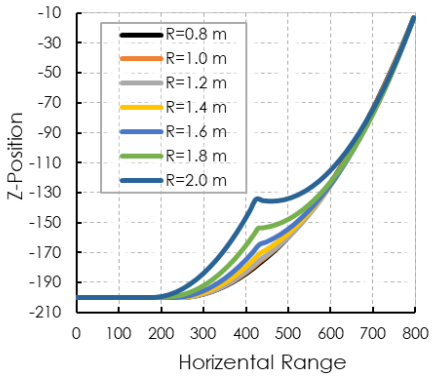

c) Buoy distance from fairlead (L) =400 m

Figure 4. Configurations of mooring lines by the effect of different buoys

4. VALIDATION

In order to calibrate the numerical model and to validate the results of ANSYS -AQWA simulation, the results of the 1:50 scaled model of OC4-DeepCwind platform laboratory test was used. The platform was tested under wind and wave load cases in Maritime Research Institute Netherlands (MARIN) in 2011 [21]. Using the results of this laboratory tested by Hall and Goupee, [4] to validate the lumped mass mooring line model. By using an NDI Certus optical motion tracking system, they were able to record the motions of the platform. The results of this validation are based on regular wave in accordance to $H_s=10.3\ [m]$ and $T_s=12.1\ (s)$ which is similar to the laboratory conditions. Figure 5 shows the ANSYS-AQWA simulation model and the laboratory model of DeepCwind platform. Shokouhian et al. [22] by employing ANSYS-AQWA software package, extracted the hydrodynamic responses of semi-submersible FOWT DeepCwind platform and validated the model with the MARIN experimental results. They explained that the average results of heave, surge, and cable tension force of the AQWA model was 15.5% closer to the test results as compared to the results of FAST program.

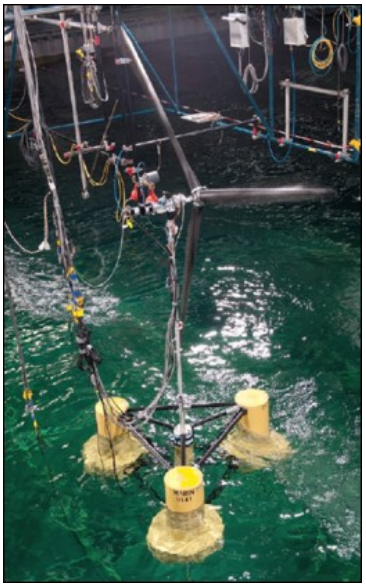

a) Scaled model of OC4-DeepCwind platform in MARIN (Goupee et al.)[4]

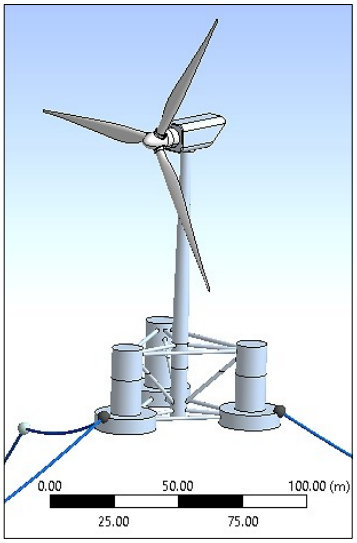

b) Simulated model of OC4-DeepCwind platform

Figure 5. Simulation and the laboratory model of OC4-DeepCwind platform

The numerical model validation is carried out in two parts: 1) Based on platform motions, and 2) Fairlead cable tension. Figure 6 illustrates the comparison between the experimental data and the ANSYS-AQWA numerical results of the platform motions for surge, heave, and pitch. Acceptable agreement in amplitudes between the numerical model and the test data is evident, although in heave and pitch motions the model predicts higher levels of excitation between the peaks. The results of the time history of fairlead point tension for test and numerical model are presented in Figure 7. The comparison shows an accuracy close to 95% between the numerical model and the experimental results. These discrepancies are assigned to the different techniques adopted in hydrodynamic simulations Such as discrepancy in the viscous-drag coefficients, Froude similarity procedure, Ignoring the effects of second-order wave forces or even difference in modeling of mooring lines.

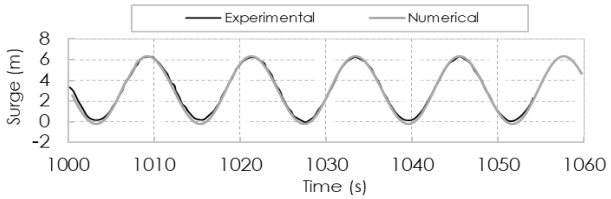

a) Surge direction

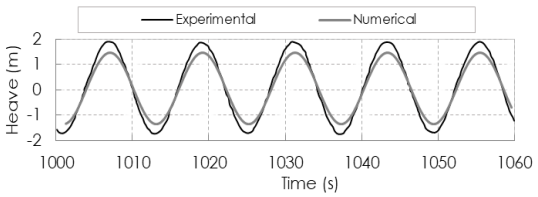

b) Heave direction

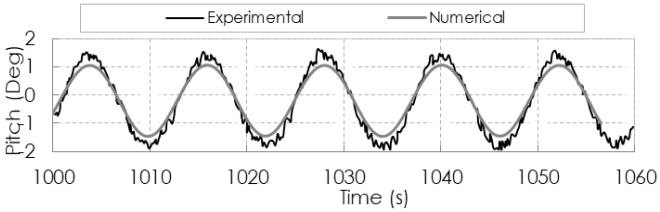

c) Pitch direction

Figure 6. Experimental and numerical comparison of platform motions

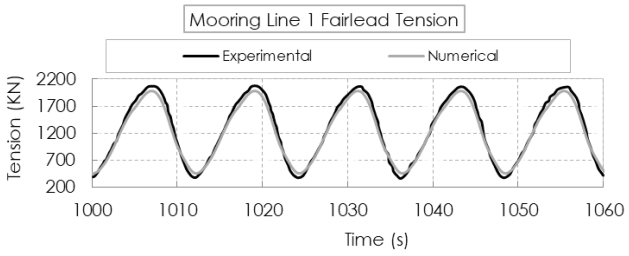

a) Fairlead tension of mooring line 1

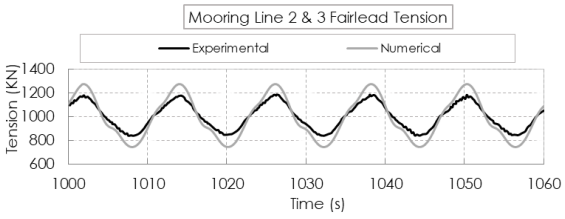

b) Fairlead tension of mooring line 2 & 3

Figure 7. Experimental and numerical comparison of fairlead tension

5. RESULTS AND DISCUSSION

In the present study, a hybrid method in ANSYS-AQWA software base on the combination of panels and Morison elements was employed to model the semi-submersible DeepCwind FOWT platform with nonlinear multi-segment catenary mooring line and intermediate buoy. The surface of full-scaled floating body is divided into 12474 quadrilateral and triangular panels. The results will be examined in three sections of mooring line's strain, tension and uplift. The mooring lines used in this study exhibit nonlinear behavior due to tension-dependent Young's modulus of the mooring chains [23]. In this regard, ANSYS-AQWA solver, analyzes the mooring lines by discretizing it into nonlinear stiffness springs, and modifying Eq. (2) into nonlinear stress-strain relationship. In this way, Van den Boom [24] showed that the tension resonance dynamics is strongly influenced by nonlinearities, due to catenary effects such as large transverse

displacements at midpoint of mooring line, elasticity and drag coefficient, thus would not be held in frequency domain models. Brown and Mavrakos [25] by studying on various systems of mooring lines, revealed that by using nonlinear time-domain methods, the mooring line tension and damping results, were generally in good agreement. In contrast, the results of frequency-domain analyze, showed large scatter and significant disagreements, in comparison to nonlinear time-domain methods especially in damping coefficient results.

According to the arrangement of the cables (Figure 3), it is expected cable 1 is exposed to a greater force than other cables due to the 0° direction (parallel to turbine hub) of wave and current incidence. Also, since the platform is symmetric about the longitudinal axis, cable 2 and 3 are also symmetrical. Therefore, only the answers for cable 2 are provided. In the next section we present and discuss the results of the strain, anchor uplift and platform motions on different buoys size and different position along the cable.

5.1. Elements strain along mooring lines

Due to elasticity properties, the cable length can be stretched due to the tensile forces caused by the movement of the platform. In fact, the strain of the cable is the non-dimensional ratio of cable elongated length to actual length of the cable ($\varepsilon = \frac{S_e - S_{e_0}}{S_{e_0}}$). Steel chains are subjected to cyclic loads, loading and offloading. Therefore, due to the low elasticity of the steel chains, permanent plastic strains occur start growing cracks at notches and eventually result in fracture. Figure 8 illustrates the variation of mooring line 1 strain under the environmental condition of the problem. As can be seen in this figure, in all buoys' placements, the strain along the cable is decreased by varying the buoy size. The larger buoy size, the lower strain along the cable and more strain drop rate. In this figure, "L" indicates the horizontal distance between the center of buoy to the fairlead point on platform. The "Original" model refers to the mooring lines of DeepCwind platform without buoy. Table 3 compares the percentage of strain reduction at the anchor and fairlead points of the cables. The results are shown that when the buoy approaches to the center of the cable, the effect of buoy on strain reduction is more evident. Placing the buoy at 300 [m] from the fairlead point has the best influence so that over 90% can help to reduce mooring lines strain.

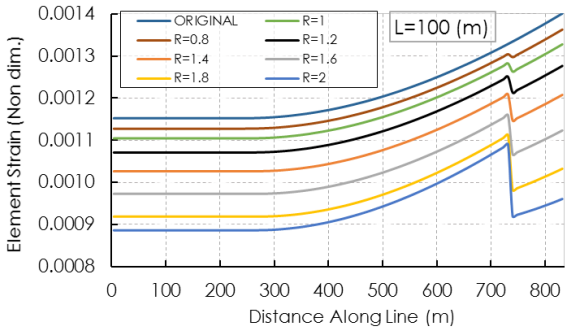

a) Bouys position at L=100 [m]

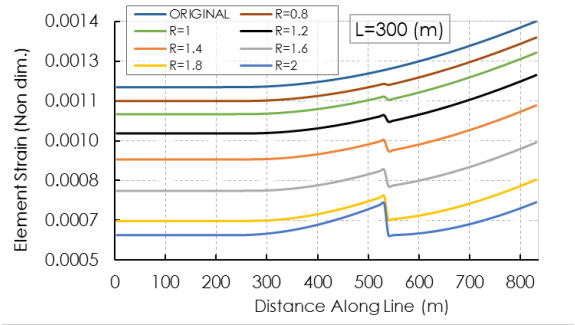

b) Bouys position at L=300 [m]

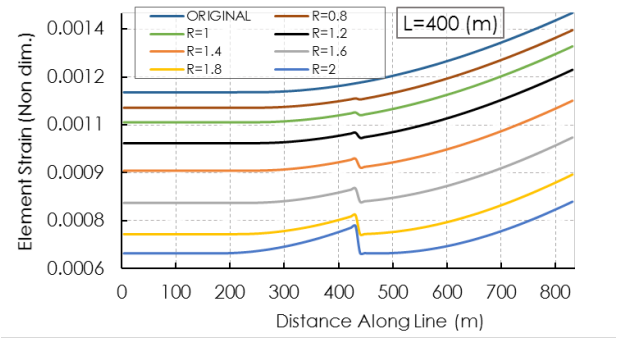

c) Bouys position at L=400 [m]

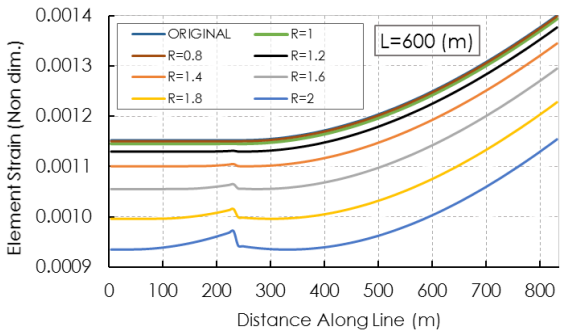

d) Bouys position at L=600 [m]

Figure 8. Variations of cable strain against different buoy positions and radiuses

Table 3. Strain reduction in each condition

Percentage of Strain Reduction at Anchor Point							
R / L	0.8	1	1.2	1.4	1.6	1.8	2
100	-2.20	-4.33	-7.59	-12.27	-18.44	-25.40	-30.00
200	-3.89	-7.87	-14.33	-24.45	-39.70	-59.43	-71.67
300	-4.76	-9.69	-17.84	-30.95	-51.28	-77.78	-93.88
400	-4.39	-8.87	-16.06	-27.08	-42.99	-62.74	-77.86
500	-2.76	-5.55	-9.95	-16.55	-25.85	-37.70	-49.16
600	-0.16	-0.58	-1.98	-4.69	-9.19	-15.67	-23.24
Percentage of Strain Reduction at Fairlead Point							
100	-2.80	-5.51	-9.74	-15.98	-24.70	-35.67	-45.80
200	-3.99	-8.09	-14.79	-25.38	-41.74	-64.40	-83.49
300	-4.58	-9.25	-16.94	-29.25	-48.36	-74.21	-94.90
400	-4.02	-8.09	-14.58	-24.42	-38.58	-56.56	-72.95
500	-2.47	-4.95	-8.86	-14.69	-22.90	-33.55	-44.93
600	-0.14	-0.51	-1.76	-4.16	-8.19	-14.07	-21.37

5.2. Tension

One of the most important parameters of mooring line design and fatigue analysis is cable tension. Tension force is defined as the tensile force applied to the mooring lines and, also the nonlinear dynamic couple between the 6 degrees of freedom platform and the mooring lines. Material properties, stress-strain relation and restoring stiffness of lines are also influential factors in predicting cable's dynamic responses [26]. Increasing applied cyclic tension loads and ramping inline tensions in mooring lines, leads to formation of crack in chains of catenary mooring lines. The tensile cracks are mostly perpendicular to the loading direction, so that when it reaches a critical length, the mooring line abruptly fails without warning [27] Connecting the buoy device increases geometric compliance and flexibility of the mooring line and is a simple way to reduce the risk of cable failure. Figure 9 shows variations of tension of cable elements against different buoy positions and radiuses. Figure 10 indicates time history of cable tension for mooring line 1,2 and 3 which are equals due to symmetry. What is evident in all the figures is the positive role of buoys in diminishing the cable tension. As the buoy size increases, the damping trend of cable fluctuations also intensifies and stabilizes. According to Figure 10, from 100 meters to 400 meters of buoy position, with rising buoy size, stimulations from the harmonic state will become a transient form. This technique eliminates cyclic oscillation and strongly reduces the risk of the fatigue failure. When the buoy dimensions promote, the thickness of the wake turbulence layer behind the buoy also increases. This increases the drag coefficient of the buoy and consequently, increases the drag force of the cable at the buoy position, which leads to

abundance cable resistance against the applied forces. Figure 11 shows the polynomial regression of mooring lines tension versus alternative buoy volumes. The positive effect of the buoy in reducing tension force is evident in all cases. The highest depreciation rates for mooring lines 2 and 3 occurred at distance of 300 [m] and at a radius of 2 [m] in which, reduces the cable tension up to 45%. Also, the effectiveness of the buoys in reducing the tension of mooring line 1 is less than mooring line 2 and 3, which at best reduces the cable tension by 30% in 400-meter buoy distance.

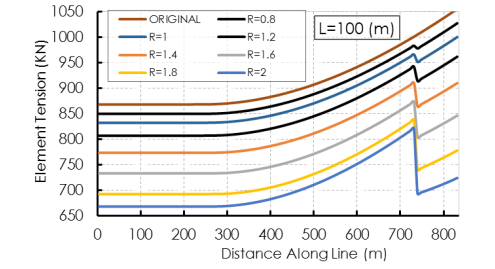

a) Bouys position at L=100 [m]

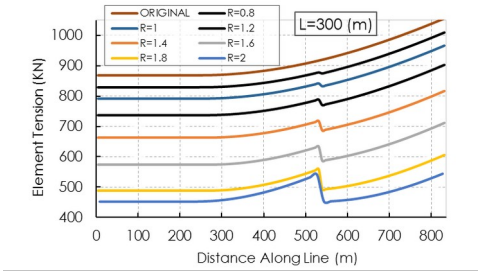

b) Bouys position at L=300 [m]

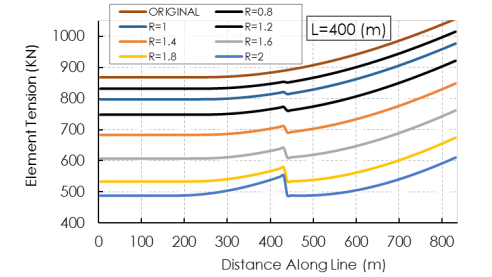

c) Bouys position at L=400 [m]

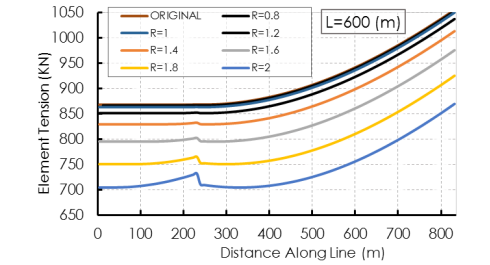

d) Bouys position at L=600 [m]

Figure 9. Variations of tension of cable elements against different buoy positions and radiuses

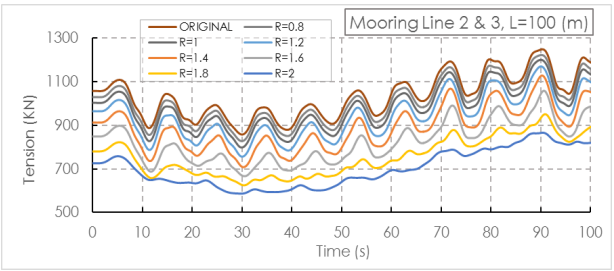

a) Effect of bouys at L=100 [m]

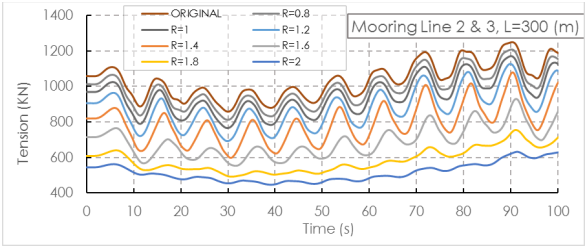

b) Effect of bouys at L=300 [m]

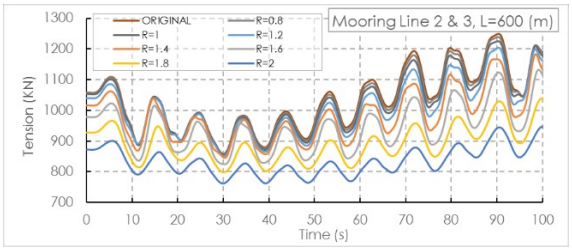

c) Effect of bouys at L=600 [m]

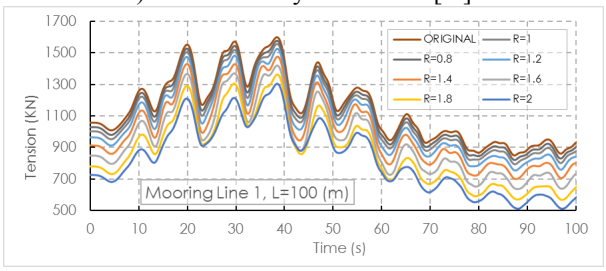

d) Effect of bouys at L=100 [m]

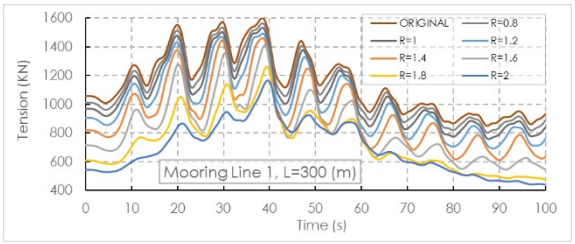

e) Effect of bouys at L=300 [m]

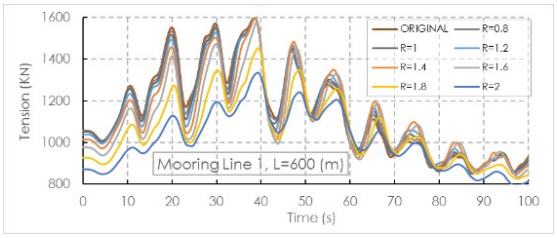

f) Effect of bouys at L=600 [m]

Figure 10. Time history of mooring lines 1,2 and 3 tension versus different buoy positions and raduises

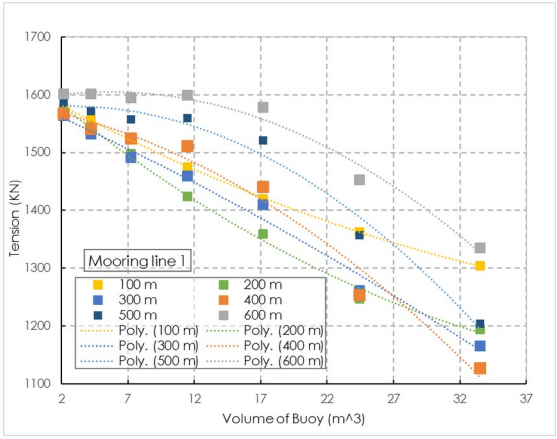

a) Polynomial regression of mooring lines 1

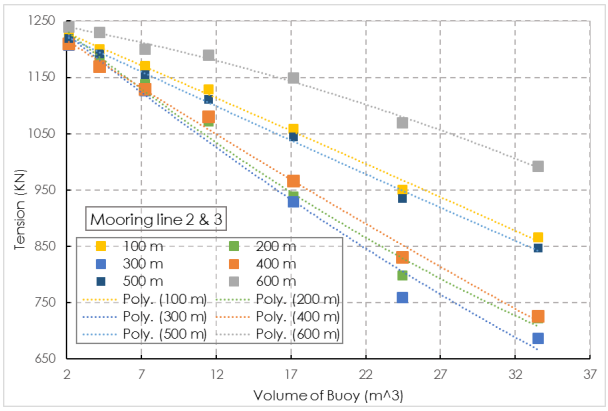

b) Polynomial regression of mooring lines 2 & 3

Figure 11. Polynomial regression of mooring lines tension versus alternative buoy volumes

5.3. Anchor uplift

The anchor uplift force is actually the vertical (upward) component of the tension force at the point of connection to the sea bed. This force is equal to the cable buoyancy force. When the buoy is attached to the mooring system, depending on the installing position, it will add positive or negative buoyancy to the attachment points. Figure 12 shows time history of anchor uplift at different position. Figure 13 summarizes the obtained results in comparison with the original mooring line configuration. The results show that from fairlead point up to 300 [m] buoy position along the cable. Due to dominance of cable and buoy's gravitational weight and inline drag term, the anchor uplift has a downward trend so that by placing the buoy with 1.8 [m] radius at distance of 200 [m], it helps to reduce the uplift force up to 70% and 95% for mooring line 1 and 2 (or 3), respectively. However, as the buoy passes 300 [m] distance, the transverse component of the tension and drag force, due to buoy and cable density, increases the vertical forces. On the other hand, the buoy will tolerate a part of the cable's weight and reduce the gravity force of the cable. In resultant, by placing buoy with radius of 2 [m] at distance of 600 [m], we observe 30-time increase in anchor uplift force. It should be noted that in order to reduce the uplift force, the laid length of the mooring line must be increase, as shown in Figure 3 and 5.

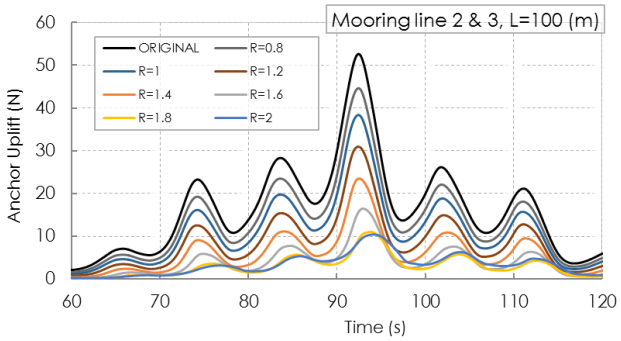

a) Effect of bouys at L=100 [m]

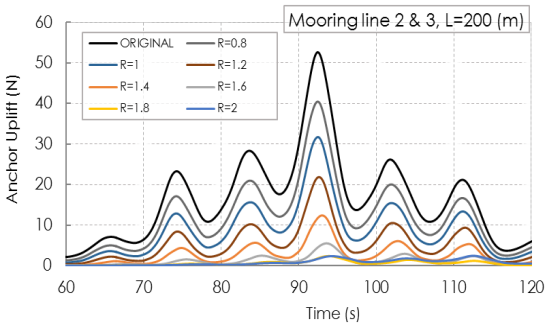

b) Effect of bouys at L=200 [m]

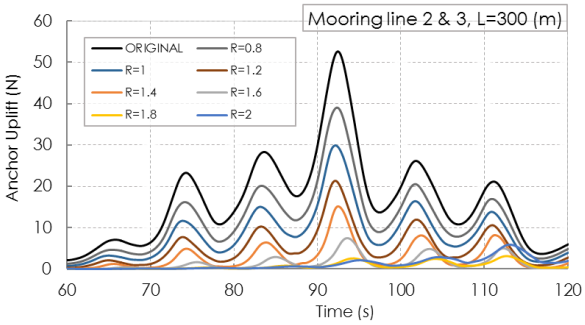

c) Effect of bouys at L=300 [m]

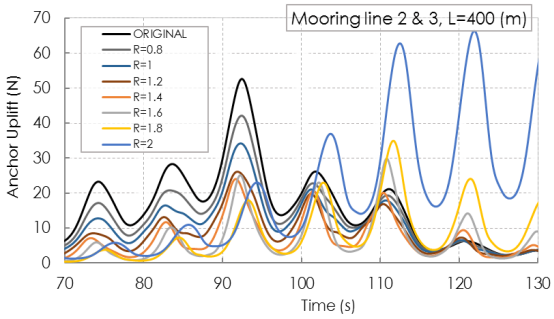

d) Effect of bouys at L=400 [m]

Figure 12. Time history of mooring line 2 & 3 uplift versus different buoy positions and raduises

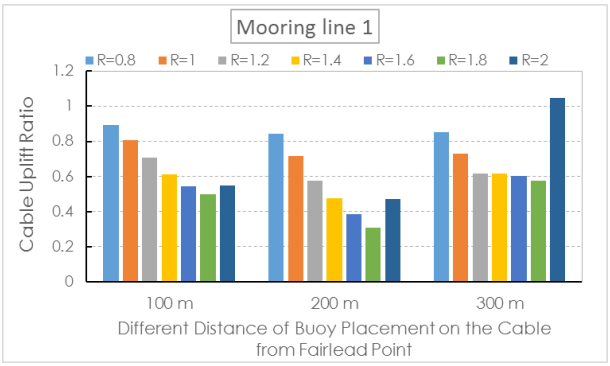

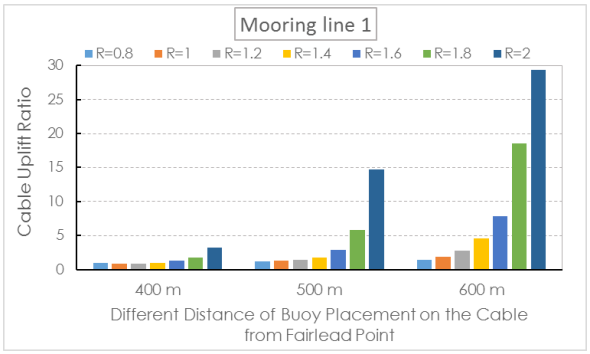

a) Mooring line 1 uplift ratios

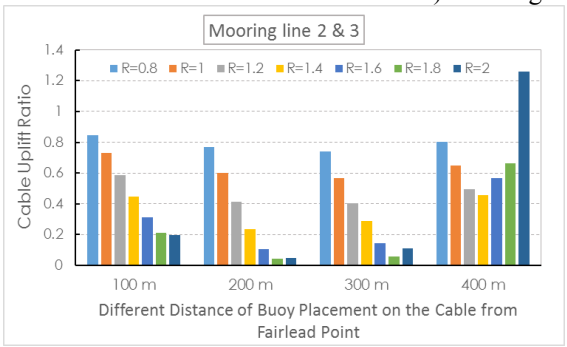

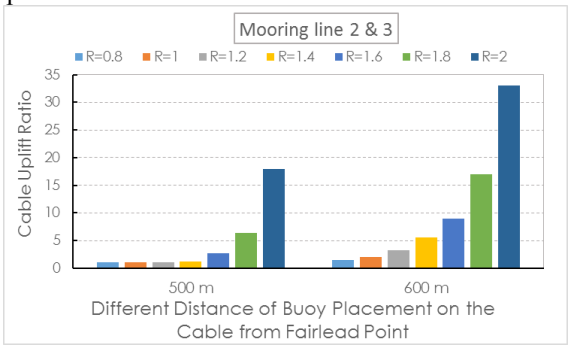

c) Mooring line 2 & 3 uplift ratios

Figure 13. Ratios of anchor uplift with bouy compared to non-buoy mode

5.4. Platform motion

Fully-coupled time-responses of OC4-DeepCwind platform (surge, heave and pitch motions at CG) where the buoy with 2 [m] radius is placed in different positions of the mooring system are shown in Figure 14. A summary of the platform motions changes under different conditions was compared to the original model and is presented in Table 4. According to Table 4, by increasing the radius of the buoy from 0.8 [m] up to 1.2 [m] at different positions, in three directions of surge, heave and pitch, there is no noticeable change in platform motions. Most of the major changes in platform motion occur with the buoy positioning between 300 and 400 meters, roughly in the middle of mooring line. Within a radius of 2 [m] for buoy, the range of motion increases to its maximum, so that within 400 meters of the buoy position, the amplitude of motion increases to 42%, 23%, and 34% in surge, heave and pitch degrees of freedom, respectively.

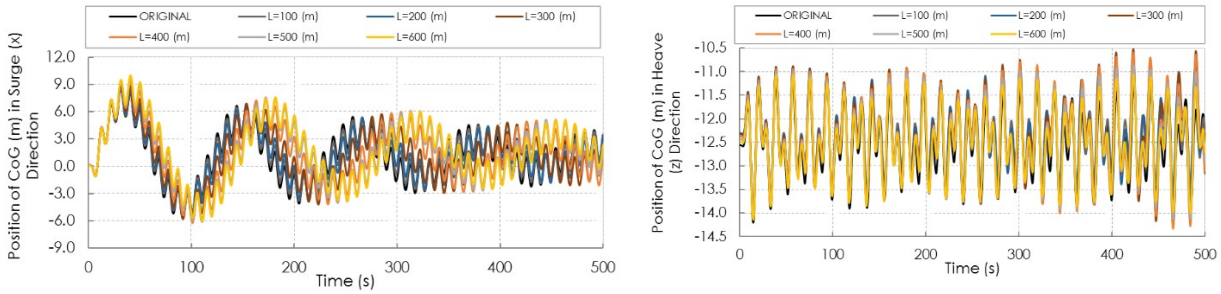

a) Surge direction

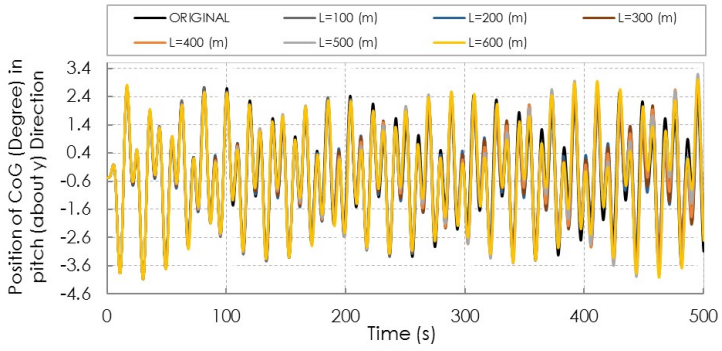

c) Pitch direction

Figure 14. Time history of motion responses in different distance of buoy placement on the cable from fairlead point

Table 4. Motion variations in each condition

Percentage of Motion Amplitude Changes Compared to Original Model							
L R	0.8	1	1.2	1.4	1.6	1.8	2.0
Surge (x)							
100	-0.28	-0.51	-0.83	-1.12	-0.62	+1.66	+5.22
200	-0.50	-0.95	-1.66	-2.07	+0.10	+5.81	+16.90
300	-0.73	-1.34	-1.98	-1.54	+5.12	+17.75	+34.19
400	-0.29	-0.47	-0.66	+1.76	+9.81	+25.22	+42.32
500	+0.64	+0.82	+2.55	+5.33	+11.62	+22.76	+37.05
600	+0.74	+1.16	+3.37	+7.14	+12.24	+20.01	+29.65
Heave (z)							
100	-0.09	-0.23	-0.29	-0.29	+0.06	+0.52	+0.99
200	-0.16	-0.29	-0.43	-0.29	+0.43	+1.55	+3.67
300	-0.16	-0.29	-0.39	-0.16	+0.82	+1.98	+20.04
400	-0.09	-0.16	-0.26	-0.23	0.+49	+3.53	+23.65
500	+0.03	0	+0.16	+0.92	+3.30	+4.13	+8.03

600	+0.06	+0.09	+0.16	+2.08	+3.07	+4.03	+5.66
Pitch (about y)							
100	-0.11	-0.08	+0.01	-0.04	-0.57	-0.79	+0.53
200	-0.23	-0.45	-0.84	-1.48	-1.90	-0.66	+11.08
300	-0.31	-0.61	-1.15	-1.87	-0.86	+2.83	+38.32
400	-0.17	-0.31	-0.54	-0.84	+3.81	+7.51	+34.09
500	+0.11	+0.18	+1.35	+3.55	+6.71	+7.93	+14.85
600	+0.11	+0.30	+0.66	+2.95	+3.71	+7.13	+14.19

6. CONCLUSIONS

This study was comprehensively investigated the mechanical behavior of DeepCwind semi-submersible FOWT platform mooring lines, nonlinear catenary cables of platform divided into two segments and intermediate buoy device attached at catenary segment joints. The tension, anchor uplift, strain at different buoy radiuses and its position along cable were presented in detail. Moreover, platform motion at three directions (heave, pitch and yaw) were analyzed. The results of the present study led to the following conclusions:

1. When the buoy device is mounted on the cable, the cable is raised positively due to the increased cable's buoyancy and bearing part of the cable weight. Larger buoy size makes higher the cable lift. Also, as the buoy gets closer to the anchor point, the angle of joint segments increases.
2. Placing the buoy within 200 to 400 [m] distance, has the most influence to reduce the strain at both fairlead and anchor points so that Enables mooring lines to reduce strain by 90%.
3. As the buoy radius increases up to 2[m], the strain decreases along the cable and the strain drop rate is greater.
4. By rising buoy radius up to 2 [m], tension stimulations from the harmonic state will become a transient form and eliminates cyclic oscillation and strongly reduces the risk of fatigue.
5. The existence of buoy at distance between 200~300 [m] has more effect on reducing the mooring line's tension rate. when the distance is 300 [m] and radius of buoy with [2], the cable tension is reduced 45%.
6. Positioning the buoy in 400 [m] up to 600 [m] horizontal distance from fairlead, will lead to a sharp increase in uplift force.
7. By increasing the radius of the buoy up to 1.2 meters at different points, there is no noticeable variation in platform motion.
8. Most of the major changes in the platform's motion are due to the approximate positioning of the buoy being in the middle of mooring line.
9. The wrong choice of buoy position can increase the platform's horizontal offset by up to 42%.
10. Taking all aspects into account, positioning the ball with a radius of 1.8 [m] at 200 [m] distance from fairlead point, has a good effect on improving the dynamic behavior of the mooring line.

CONFLICT OF INTEREST

The authors declare no potential conflict of interests.

AUTHOR CONTRIBUTIONS

Mohammad Motallebi: Conceptualization; Methodology; Software; Validation; Visualization; Writing-original draft.

Hassan Ghassemi: Supervision; Conceptualization; Data Analysis; Methodology; Software; Validation; Visualization; Writing-original draft.

DATA AVAILABILITY STATEMENT

The data that support the findings of this study are available from the corresponding author upon reasonable request.

ORCID

Hassan Ghassemi: https://orcid.org/0000-0002-6201-346X

REFERENCES

1. Y. H. Bae, M. H. Kim, and H.-C. Kim, "Performance changes of a floating offshore wind turbine with broken mooring line," *Renewable Energy,* vol. 101, pp. 364-375, 02/01 2017.
2. H. Sabziyan, H. Ghassemi, F. Azarsina, and S. Kazemi, "Effect of Mooring Lines Pattern in a Semi-submersible Platform at Surge and Sway Movements," *Journal of Ocean Research,* vol. 2, pp. 17-22, 10/09 2014.
3. I. Martinez, A. Constantinescu, P. Bastid, Y. Zhang, and V. Venugopal, "Computational fatigue assessment of mooring chains under tension loading," *Engineering Failure Analysis,* vol. 106, 08/01 2019.
4. M. Hall and A. Goupee, "Validation of a lumped-mass mooring line model with DeepCwind semisubmersible model test data," *Ocean Engineering,* vol. 104, pp. 590-603, 08/01 2015.
5. J. Azcona, X. Munduate, L. González, and T. Nygaard, "Experimental validation of a dynamic mooring lines code with tension and motion measurements of a submerged chain," *Ocean Engineering,* 11/15 2016.
6. M. Karimi, B. Buckham, and C. Crawford, "A fully coupled frequency domain model for floating offshore wind turbines," *Journal of Ocean Engineering and Marine Energy,* vol. 5, no. 2, pp. 135-158, 2019/05/01 2019.
7. J. Yu, S. Hao, Y. Yu, B. Chen, S. Cheng, and J. Wu, "Mooring analysis for a whole TLP with TTRs under tendon one-time failure and progressive failure," Ocean Engineering, vol. 182, pp. 360-385, 2019/06/15/ 2019.
8. K. Lee, H.-S. Han, and S. Park, "Failure analysis of naval vessel's mooring system and suggestion of reducing mooring line tension under ocean wave excitation," Engineering Failure Analysis, vol. 57, pp. 296-309, 11/01 2015.
9. A. Robertson *et al.*, "Definition of the Semisubmersible Floating System for Phase II of OC4," United States2014-09-01 2014, Available: https://www.osti.gov/servlets/purl/1155123.
10. W. Dongjiao, "Static analysis of a wire rope-chain- buoy/sinker mooring line," *China Offshore Platform,* vol. 6, p. 003, 2007.
11. D. Qiao, J. Yan, and J. Ou, "Effects of mooring line with buoys system on the global responses of a semi-submersible platform," *Brodogradnja,* vol. 65, pp. 79-96, 03/01 2014.
12. H. Ghafari and M. Dardel, "Parametric study of catenary mooring system on the dynamic response of the semi-submersible platform," *Ocean Engineering,* vol. 153, 04/01 2018.
13. C. Kwan and F. Bruen, "Mooring line dynamics: comparison of time domain, frequency domain, and quasi-static analyses," presented at the Offshore Technology Conference, Houston, Texas, 6-9 May, 1991.
14. Z.-M. Yuan, A. Incecik, and C. Ji, "Numerical study on a hybrid mooring system with clump weights and buoys," *Ocean Engineering,* vol. 88, pp. 1–11, 09/01 2014.
15. D. Dessi, A. Carcaterra, and G. Diodati, "Experimental investigation versus numerical simulation of the dynamic response of a moored floating structure to waves," *Proceedings of the Institution of Mechanical Engineers, Part M: Journal of Engineering for the Maritime Environment,* vol. 218, no. 3, pp. 153-165, 2004/09/01 2004.

16. A. J. Coulling, A. J. Goupee, A. N. Robertson, J. M. Jonkman, and H. J. Dagher, "Validation of a FAST semi-submersible floating wind turbine numerical model with DeepCwind test data," Journal of Renewable and Sustainable Energy, vol. 5, no. 2, p. 023116, 2013/03/01 2013.
17. A. Goupee, M. Fowler, R. Kimball, J. Helder, and E. Ridder, "Additional Wind/Wave basin testing of the DeepCwind semi-submersible with a performancematched wind turbine.," in *Proceedings of the 33rd International Conference on Ocean, Offshore and Arctic Engineering*, San Francisco, California, USA, 2014.
18. Z. Liu, Y. Fan, W. Wang, and G. Qian, "Numerical Study of a Proposed Semi-Submersible Floating Platform with Different Numbers of Offset Columns Based on the DeepCwind Prototype for Improving the Wave-Resistance Ability," Applied Sciences, vol. 9, p. 1255, 03/25 2019.
19. H. Imani, M. Abbaspour, M. R. Tabeshpour, and M. Karimirad, "Effects of motion and structural vibration–induced loadings on the coupled dynamic response of a mono-column tension-leg-platform floating wind turbine," Proceedings of the Institution of Mechanical Engineers, Part M: Journal of Engineering for the Maritime Environment, vol. 234, no. 2, pp. 426-445, 2020/05/01 2019.
20. Z. Gao and T. Moan, "Mooring system analysis of multiple wave energy converters in a farm configuration," 09/10 2009.
21. M. Masciola, A. Robertson, J. Jonkman, A. Coulling, and A. Goupee, "Assessment of the importance of mooring dynamics on the global response of the DeepCwind floating semisubmersible offshore wind turbine," *Proceedings of the International Offshore and Polar Engineering Conference,* pp. 359-368, 01/01 2013.
22. M. Shokouhian, M. Head, J. Seo, W. Schaffer, and G. Adams, "Hydrodynamic response of a semi-submersible platform to support a wind turbine," *Journal of Marine Engineering & Technology,* pp. 1-16, 2019.
23. A. Tahar and M. H. Kim, "Coupled-dynamic analysis of floating structures with polyester mooring lines," *Ocean Engineering,* vol. 35, pp. 1676-1685, 12/01 2008.
24. H. Van den Boom, "Dynamic behavior of mooring lines," in BOSS Conference, Delft,The Netherlands, 1985.
25. D. Brown and S. Mavrakos, "Comparative study on mooring line dynamic loading," *Mar. Struct. ,* vol. 12, pp. 131-151, 1999.
26. Y.-g. Tang, S.-x. Zhang, R.-y. Zhang, and H.-x. Liu, "Development of study on the dynamic characteristics of deep water mooring system," *Journal of Marine Science and Application,* vol. 6, no. 3, pp. 17-23, 2007/09/01 2007.
27. R. D. Cook and W. C. Young, *Advanced Mechanics of materials*, Second edition ed. New Jersey: Prentice Hall, 1999